CORA Cork Open Research Archive
Cartlann Taighde Oscailte Chorcaí

Title	Modelling of a tubular kirigami (RC-kiri) with outside lamina emergent torsional joints
Authors	Ye, Siyuan;Zhao, Pengyuan;Li, Shiyao;Kavousi, Fatemeh;Hao, Guangbo
Publication date	2023-04-16
Original Citation	Ye, S., Zhao, P., Li, S., Kavousi, F. and Hao, G. (2023) 'Modelling of a tubular kirigami (RC-kiri) with outside lamina emergent torsional joints', in Laribi, M. A., Nelson, C. A., Ceccarelli, M. and Zeghloul, S. (eds) New Advances in Mechanisms, Transmissions and Applications. MeTrApp 2023. Mechanisms and Machine Science, 124, pp. 264-276. Springer, Cham. doi: 10.1007/978-3-031-29815-8_26
Type of publication	Article (peer-reviewed);Conference item;Book chapter
Link to publisher's version	10.1007/978-3-031-29815-8_26
Rights	© 2023, the Authors. Published by Springer Nature Switzerland AG. This is a post-peer-review, pre-copyedit version of a paper published in Laribi, M. A., Nelson, C. A., Ceccarelli, M. and Zeghloul, S. (eds) New Advances in Mechanisms, Transmissions and Applications. MeTrApp 2023. Mechanisms and Machine Science, vol 124. Springer, Cham. The final authenticated version is available online at: https://doi.org/10.1007/978-3-031-29815-8_26
Download date	2026-11-06 02:53:35
Item downloaded from	https://hdl.handle.net/10468/14686



University College Cork, Ireland
Coláiste na hOllscoile Corcaigh

Modelling of a tubular kirigami(RC-kiri) with outside lamina emergent torsional joints

Siyuan Ye[1 [0000−0003−0244−7407]], Pengyuan Zhao[1,2 [0000−0002−1645−191X]], Shiyao Li[1 [0000−0003−2489−8524]], Fatemeh Kavousi[1 [0000−0002−4166−4589]], and Guangbo Hao[1 [0000−0002−5930−5453]]

[1] School of Engineering and Architecture
University College Cork, T12 K8AF, Ireland
g.hao@ucc.ie
[2] Shenyang Institute of Automation Chinese Academy of Sciences, 110016, Shenyang, Liaoning, China

Abstract. This paper applies the traditional kirigami technique to the non-rigid-foldable tubular origami, which provides a new method to convert the non-rigid foldability. Tubular Yoshimura and Kresling origami, as two typical non-rigid-foldable structures, are applied with the kirigami technique and presented. A radially closable origami (RC-ori) becomes a rigid-foldable kirigami (RC-kiri) when cutting the connected edges of every folding unit.
The creases of RC-kiri are applied with outside LET joints, and the simulated model is constructed and analysed by Abaqus. The force-displacement relationship is obtained which shows two stages divided by the critical instability point. The FEA results are compared with the theoretical results, and its potential sources of errors are analysed. A physical model is made by 3D printing. The verification methods including dihedral angles, diameter-displacement curves, and force-displacement curves in outward folding configuration. Our study builds a bridge between origami and kirigami and expands the application of LET joints to the fabrication of tubular kirigami.

Keywords: Tubular kirigami · Non-rigid foldability · Outside LET joint · Finite element analysis · 3D print.

1 Introduction

Tubular origami such as Kresling, waterbomb, and Yoshimura has become an emerging topic over the recent decades. Their properties have great potential in a wide range of applications. Their tubular shape provides a closed environment for medical devices [1], pneumatic actuators [2], and omnidirectional robot arms [3]. Their non-rigid foldability benefits energy absorbers [4]. Metamaterials exploit their tunable mechanical response properties [5]. With their radial closability, their application even extends to valves [6].

A large class of tubular origami is non-rigid-foldable [7, 8], which greatly limits its fabrication and applications. Its folding requires the in-plane deformation or the travelling of hinges [9]. The current common solution is to use flexible materials for the in-plane deformation. Bulter et al. tested five kinds of flexible sheet materials for the

origami bellows used in Mars rovers [10]. Melancon et al. 3D printed an inflatable Kresling structure with the flexible TPU95A filament and coated it with a thin layer of polydimethylsiloxane (PDMS) [11]. Flexible materials such as paper and plastic sheets are easy to deform, while most engineering materials are too rigid to allow large deformations. Therefore, a new method is applied in this paper to convert the non-rigid foldability.

Most tubular origami structures are built by isometrically embedding folding patterns in 3D space [8]. Non-rigid foldability comes from the over-constrained connections between each folding unit, as vertex positions conflict when defined by the motion of different folding units [12]. According to this feature, cutting the connected edges can change the non-rigid foldability. And this approach makes the structure a kirigami. Kirigami is popular in recent research for its high stretchability and deformability [13, 14], but few researchers have applied kirigami techniques to origami structures for research. This paper takes a radially closable tubular origami pattern (RC-ori) as the main object [6], and modelling and analysing are demonstrated based on its kirigami configuration(RC-kiri).

Folding along the creases of engineering materials is a great challenge. A fold is a reduction in stiffness along the creases [15]. For thin materials with high flexibility, folding at the crease can be achieved by plastic deformation or punching [10, 16–18]. However, to withstand loads and insulate heat, radiation, and sound, the thickness and stiffness of engineering materials should be considered [19]. High stiffness strongly limits the possible folding motions [20]. In addition, engineering materials always require the assembly of additional mechanical hinges or membranes [21]. For instance, Lang et al. applied the synchronized-offset rolling-contact elements (SORCE) to thick origami mechanisms [22]. Bulter et al. proposed a regional sandwiching of compliant sheets (ReCS) technique [23].

The compliant joint has been the focus of many studies over the years [24, 25]. It allows the material to maintain stiffness on the panels while reducing stiffness at the creases without adding additional hinges or membranes, which is an effective way to surrogate folds [20, 21]. Delimont et al. summarized and evaluated several commonly used compliant joints [15, 26]. Xie et al. designed a new outside-deployed lamina emergent joint for a large angular rotation [27]. Ferrell et al. developed a revolute U-form flexure (RUFF) and a torsional U-form flexure (TUFF) for use in sheet metals [28]. Wilding et al. designed three kinds of LET joints that have minimal parasitic motion under tension and compression [29]. To simplify the model, this paper applies the most commonly used outside LET joints to tubular kirigami.

The paper is organized as follows. In section 2, the kirigami technique is applied to Kresling, Yoshimura, and RC-ori, their different configurations are presented. And the kinematic analysis is performed on RC-kiri. Section 3 applies the outside LET joint to the tubular RC-kiri. The configuration design, theoretical modelling, and force-displacement relationship analysis is carried out. In Section 4, the finite element model is briefly described, and the FEA results are compared with the theoretical results. Verification is performed to verify the accuracy of the results. And the paper concludes in Section 5.

2 Tubular kirigami

2.1 Yoshimura and Kresling kirigami

Most kirigami are planar structures [30–33], and to the best of our knowledge, spatial kirigami is mainly studied by its tensile motion [13, 34, 35]. This paper, however, analyses the motion generated by compressing the tubular kirigami. Typical non-rigid-foldable tubular origami structures (Kresling and Yoshimura) are applied with the kirigami technique and analysed below.

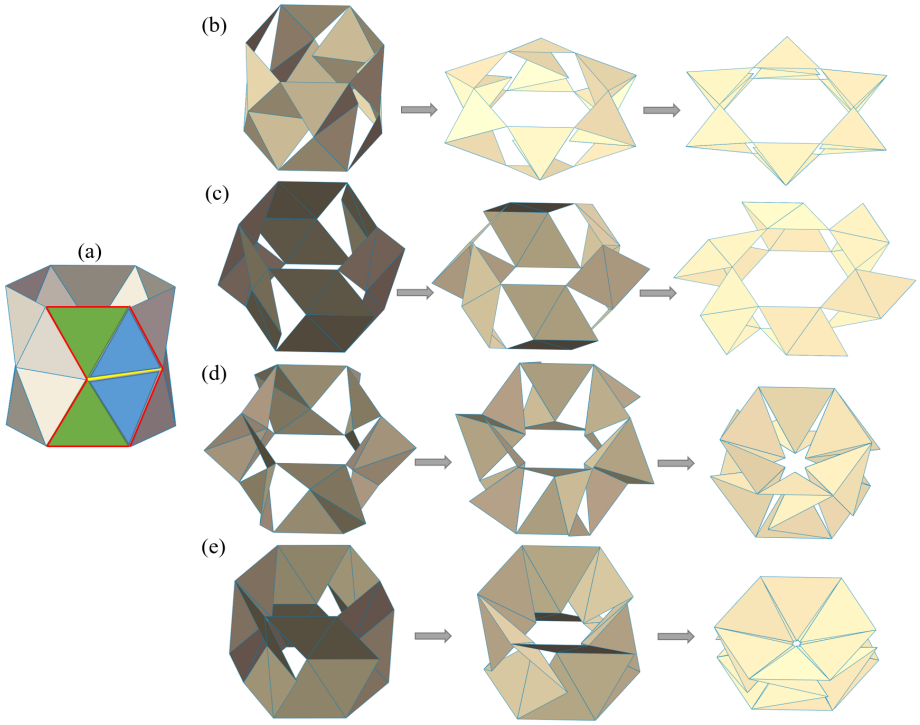


Fig. 1. (a) Tubular Yoshimura structure. (b-e) The folding process of four configurations of tubular Yoshimura kirigami structure.

Several conditions need to be clarified here. First, to keep the ends shape(polygon) during folding, a symmetrical stacking of two layers is necessary. Second, the folding state of every folding unit is the same, so that there is only one degree of freedom. Folding units are the embedded units that make up the cylinder, they have the same folding pattern. As can be seen in the Yoshimura structure (Fig. 1a), one of the folding units is marked by red lines. There are four triangle facets of each folding unit and they are symmetrical along the yellow line in the middle. When the connected edges between each folding unit are cut, the green facets and blue facets both can be folded inward or outward. The structure becomes rigid-foldable and that leads to four configurations of Yoshimura kirigami, as shown in Fig. 1(b-e).

Similar to Yoshimura, Kresling also becomes rigid-foldable when its connected edges are eliminated. However, some Kresling and Yoshimura kirigami structures only has three configurations because panel interference occurs when all facets are folded inwards. In fact, the single-layer folding unit of both Yoshimura and Kresling patterns is a parallelogram composed of two identical triangles. Yoshimura uses isosceles triangles [36], and Kresling generally uses obtuse triangles. Thus, the triangle parameters seriously affect the structure properties. Meanwhile, another important parameter is the number of folded units. Fig. 1 only takes the equilateral triangle with six units as an example.

2.2 Radially closable kirigami (RC-kiri)

RC-ori is a radially closable origami with non-rigid foldability whose folding unit consists of two right-angled trapezoids and two right triangles, as shown in Fig. 2. Based on the authors' previous paper [6], the RC-ori crease pattern is fully defined by two parameters, the number of folding unit n and the polygon side length a. The side length only affects the structure size, which means the number of folding unit can fully define the configuration. This paper takes $n = 6$ as the research object because two main factors are considered. First, the cross-sectional area of the tube expands with the increase of n, and a larger cross-sectional area results in a greater adjustable range [6]. Second, when comparing the layers of overlapping panels in the fully folded state. It shows that there are fewer overlapping panels when $n \leq 6$, which is beneficial for fabrication. (Fig. 3)

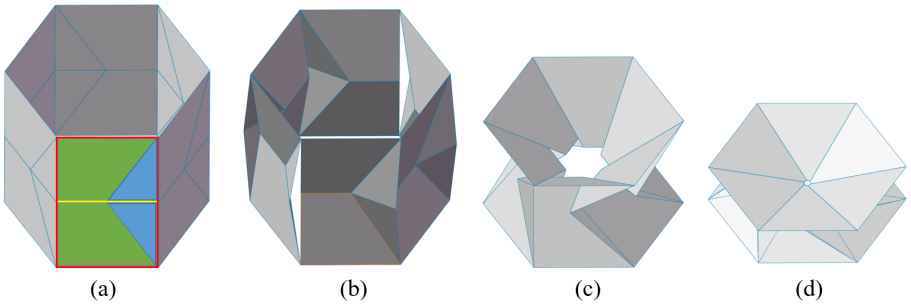


Fig. 2. The folding process of the RC-kiri structure [6]

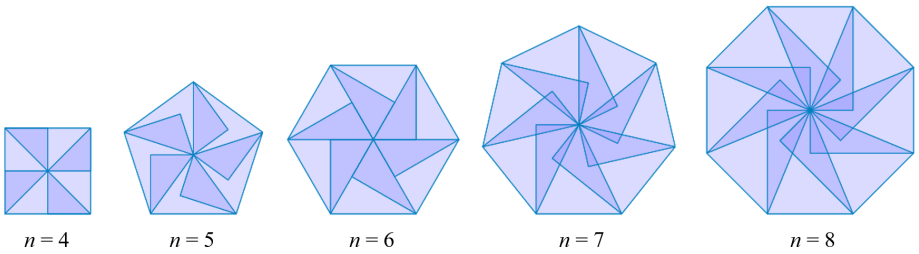


Fig. 3. The top view of fully folded RC-kiri when $n = 4, 5, 6, 7, 8$. Darker areas represent more overlapping layers.

When applying the kirigami technique to RC-ori, it becomes rigid-foldable with three configurations (Fig. 2(b-d)). When the trapezoid facets are folded inwards and the triangle facets are folded outwards, a radially closable kirigami configuration is created, and every folding unit is a degree-four vertex pattern, as shown in Fig. 4b. They have good performance because the vertex is straight-minor ($\alpha_1 + \alpha_2 = \alpha_3 + \alpha_4 = \pi$) [22].

The relationship between displacement H and the folding angle of every facet $\Delta\gamma_{\mathrm{i}}$ can be derived by the following equations,

$$\sin\beta = \frac{h}{h_0} = \frac{a\tan\theta - H}{a\tan\theta} \tag{1}$$

$$\theta = \frac{\pi}{2} - \frac{\pi}{n} \tag{2}$$

where β is half of the dihedral angle between two symmetrical trapezoid facets, h is the axial length during folding and h_0 is the initial axial length, a is the side length of every folding unit, θ is the base angle of the right-angled trapezoid and is also half of the polygon interior angle.

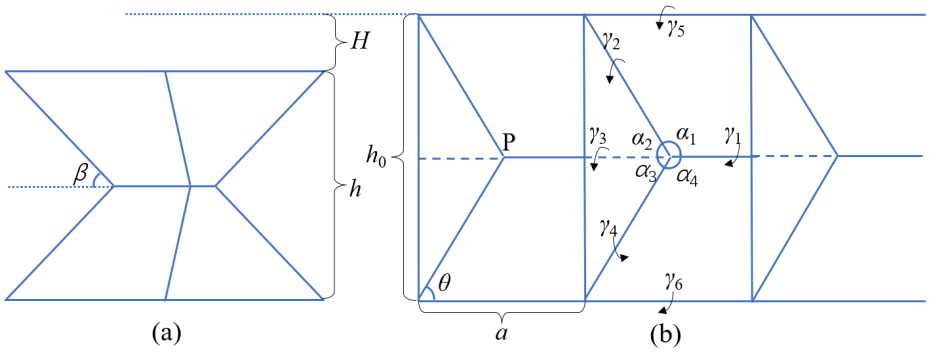


Fig. 4. (a) Front view of the RC-kiri structure. (b) RC-ori crease pattern.

Thus, the folding angle of two trapezoid facets $\Delta\gamma_1$ is obtained,

$$\Delta\gamma_1 = \pi - 2\beta = \pi - 2\arcsin\left(\frac{a\tan\theta - H}{a\tan\theta}\right) \tag{3}$$

The relationship between every folding angle is mentioned in many papers [20, 37–39],

$$\frac{\tan\frac{1}{2}\Delta\gamma_2}{\tan\frac{1}{2}\Delta\gamma_1} = \frac{\sin\frac{1}{2}(\alpha_1+\alpha_2)}{\sin\frac{1}{2}(\alpha_1-\alpha_2)} \tag{4}$$

where the angles around the degree-4 vertex α_{i} can be derived from θ, thus,

$$\Delta\gamma_2 = 2\arctan\left(\frac{\tan\frac{1}{2}\Delta\gamma_1}{\cos\theta}\right) \tag{5}$$

$$\Delta\gamma_3 = \Delta\gamma_1 \tag{6}$$

$$\Delta\gamma_4 = \Delta\gamma_2 \tag{7}$$

$$\Delta\gamma_5 = \Delta\gamma_6 = \left(\frac{\pi}{2} - \beta\right) \tag{8}$$

Here, $\Delta\gamma_5$ and $\Delta\gamma_6$ are the folding angles between the trapezoid facet and the ends extension facet. It can be seen from Fig. 5a that the two ends are lengthened to ensure every folding unit is evenly stressed.

3 Design and modelling of RC-kiri with outside LET joints

This paper applies commonly used outside LET joints to every crease of the tubular RC-kiri. Every folding unit has eight joints, as shown in Fig. 5b. To simplify the model, most of the geometric parameters of the joints are identical, the only difference is the length of the two oblique joints L_{T2} is twice that of the horizontal joints L_{T1}. The parameters are labelled in Fig. 5b and their values are listed in Table 1 (t is the thickness).

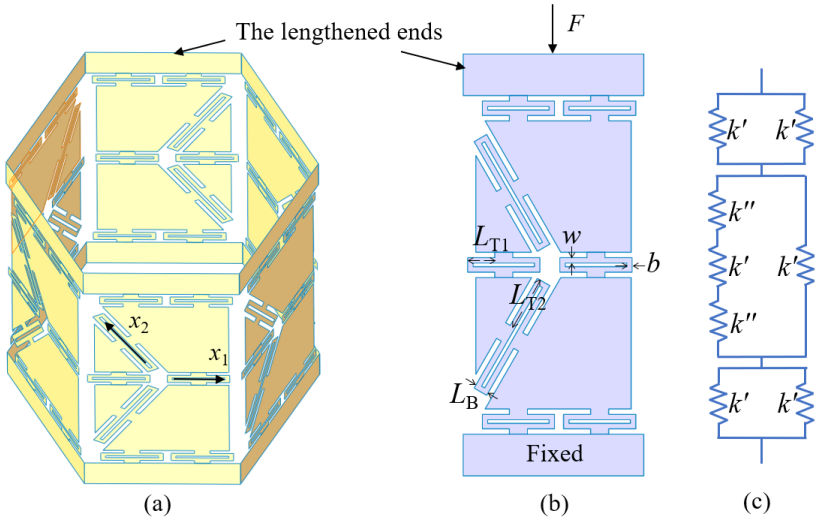


Fig. 5. (a) The tubular RC-kiri model with outside LET joints. (b) Marks for folding unit related parameters. (c) Equivalent spring model of a folding unit.

Table 1. Geometric parameters of the outside LET joints and related material parameters.

w/mm	t/mm	L_{T1} /mm	L_{T2}/mm	L_B/mm	b /mm	v	E/MPa	θ/rad	a/mm
1.5	0.8	7.5	15	4	1.5	0.37	2960	$\pi/3$	50

The folding units are indirectly connected by the extension ends. One end is fixed and the other end is applied with force. The theoretical force-displacement relationship consists of two stages, divided by the critical instability point. Before the force reaches a critical point, the structure undergoes a small displacement due to the parasitic motion of the compliant joint. When the force reaches the critical point, the panels lose stability

and folds, causing large displacements. During the folding process, the parasitic motion is not considered in theoretical model.

Before reaching the critical point, the main parasitic motion is the compression of LET joints. The stiffness is provided by Chen et al. [40], and the equivalent spring model of the folding unit is shown in Fig. 5c.

$$\frac{F}{\Delta y} = \frac{12EI_1}{L^3} \tag{9}$$

$$I_1 = \frac{tw^3}{12} \tag{10}$$

The stiffness of a horizontal joint is,

$$k' = \frac{Etw^3}{L_{\mathrm{T1}}^3} \tag{11}$$

The stiffness of an oblique joint is,

$$k'' = \frac{Etw^3}{L_{\mathrm{T2}}^3 \cos^2\theta} \tag{12}$$

The stiffness of the whole structure is,

$$k_{\mathrm{total}} = \frac{2k'^2 + 2k'k''}{4k' + 3k''} \times 6 \tag{13}$$

After reaching the critical point, the energy method is applied to find the force-displacement relationship. Since the folding is mainly about the rotational motion around the x-axis of the joint, the energy generated by the joint's torsional deformation is,

$$U = \frac{1}{2} k_{\theta \mathrm{x_i}} \Delta\theta_{\mathrm{x_i}}^2 \tag{14}$$

The equal stiffness of the outside LET joints is provided by [41,42],

$$k_{\mathrm{eq}} = \frac{2K_{\mathrm{B}}K_{\mathrm{T}}}{K_{\mathrm{T}} + 2K_{\mathrm{B}}} \tag{15}$$

$$K_{\mathrm{T}} = \frac{\omega t^3 \left(\frac{1}{3} - 0.21\frac{t}{\omega}\left(1 - \frac{t^4}{12\omega^4}\right)\right) G}{L_{\mathrm{T}}} \tag{16}$$

$$K_{\mathrm{B}} = \frac{EI_2}{L_{\mathrm{B}}} \tag{17}$$

$$I_2 = \frac{bt^3}{12} \tag{18}$$

When substituting the folding angles $\Delta\gamma_{\mathrm{i}}$ and the equal stiffness k_{eq} to Eq. (14) and differentiating it, the relationship between theoretical force and displacement during folding is obtained. Thus, the critical instability force is obtained and can be applied to Eq. (9) for the small displacement Δy. Therefore, the theoretical energy-displacement curve and force-displacement curve are obtained (see the black dotted line of Fig. 6).

4 FEA results and verification

The simulation is performed by Abaqus explicit dynamic analysis. One tube end is fixed and the other end is given a displacement. At the same time, a small inward instantaneous moment is applied to every trapezoid facet to imitate the disturbance. The folding process of the simulation model is shown in Fig. 7a. The deformation mainly occurs on the joints, which is as expected.

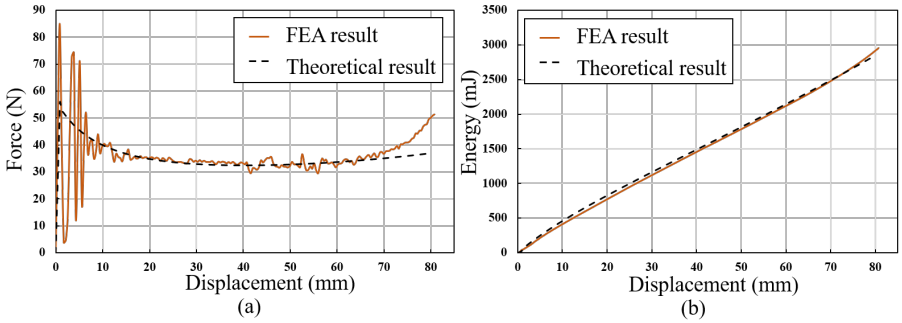


Fig. 6. (a) Force-displacement curves of both theoretical result and simulation result of inward folding RC-kiri. (b) Energy-displacement curves of inward folding RC-kiri.

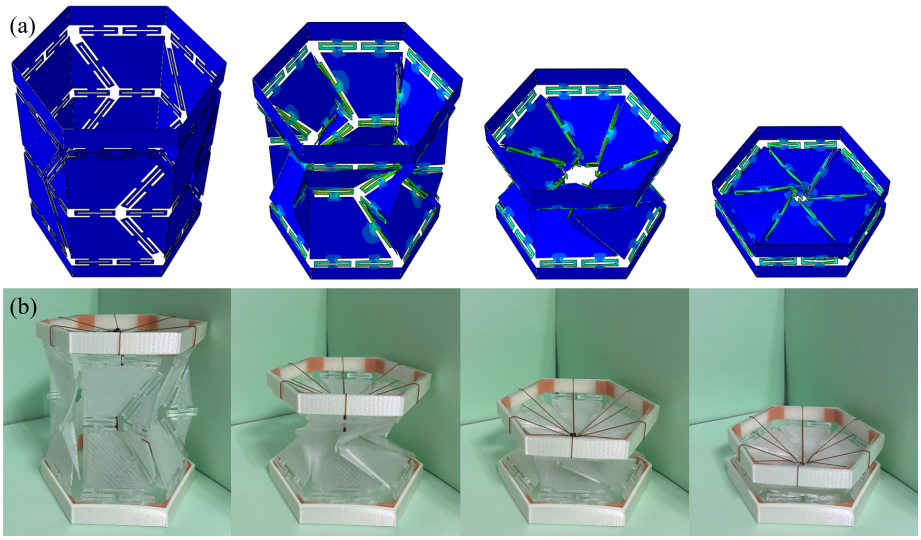


Fig. 7. (a) The inward folding process of the RC-kiri simulation model. (b) The inward folding process of the 3D printed model. (video)

The FEA simulated results are compared with the theoretical results as can be seen from Fig. 6. At the start of folding, the curve fluctuates greatly, and at the end of folding, the curve shifts. Multiple potential sources of error are identified: a) At the start of folding, the triangle facets intend to fold inward, though they change the direction because of the resistance when contact with trapezoid facets, as can be seen in Fig. 8b. b) The

applied instantaneous moment cannot imitate natural disturbance. c) Parasitic motion is not considered in the theoretical model. d) Plastic deformation occurs because of the large rotation angles. e) The thickness of the structure causes the compression stress between panels. f) The parameter settings of Abaqus software.

To verify the accuracy of the results. The dihedral angles between each facet are compared in Fig. 8. Overall the curves are consistent, except that the $\Delta\gamma_3$ is intended to fold inwards at the start and $\Delta\gamma_2$ and $\Delta\gamma_4$ undergo parasitic motions. Meanwhile, a physical model is also made using a Ultimaker 3D printer, with a PP filament which has high flexibility, as shown in Fig. 7b. Its diameter during folding is measured and compared with theoretical results and FEA results, as shown in Fig. 9. The diameter determines the cross-sectional area, which indicates the feasibility of adjusting the cross-sectional area by controlling the displacement.

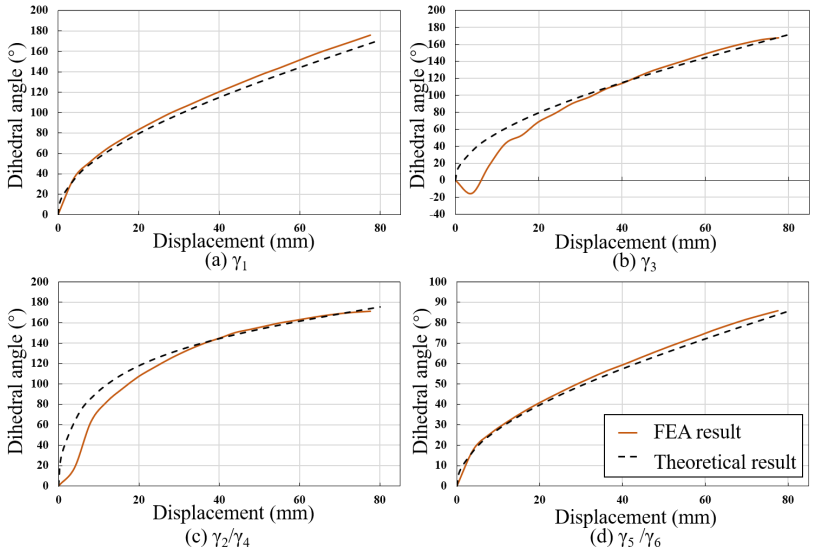


Fig. 8. The dihedral angles between each facet.

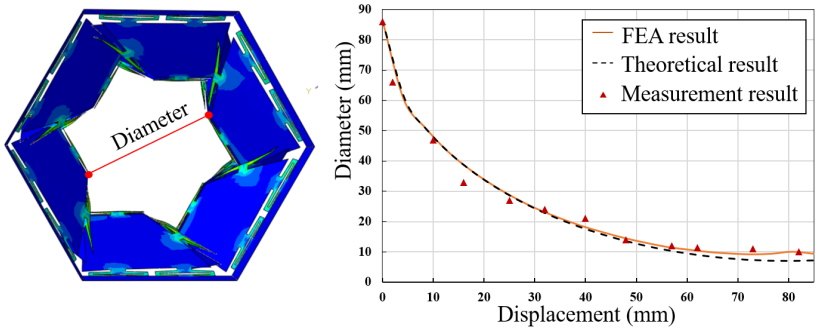


Fig. 9. (a) Top view of the simulation model, the diameter is the distance between the central point P of two opposite folding units. (b) The diameter-displacement curves during folding.

There are three configurations of RC-kiri, and only two configurations caused by natural disturbance are considered in this paper. In addition to the aforementioned inward folding, the outward folding process is shown in Fig. 10. In this configuration, the oblique joints should not contribute the movement of the overall structure, which makes the RC-kiri similar to a Sarrus linkage. However, it can be seen from the simulation model that significant parasitic movement occurs at the oblique joints. The curves shown in Fig. 11 are in good agreement except some fluctuation mainly due to the parasitic motion.

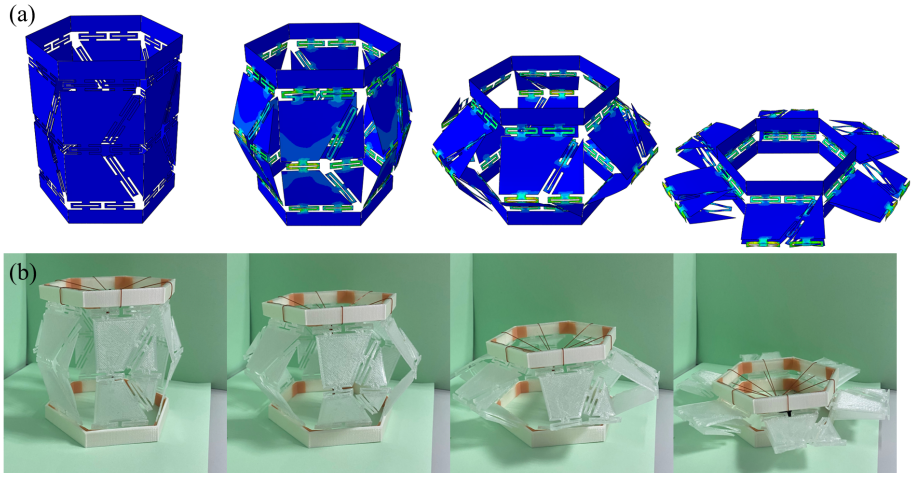


Fig. 10. (a) The outward folding process of the RC-kiri simulation model. (b) The outward folding process of the 3D printed model.

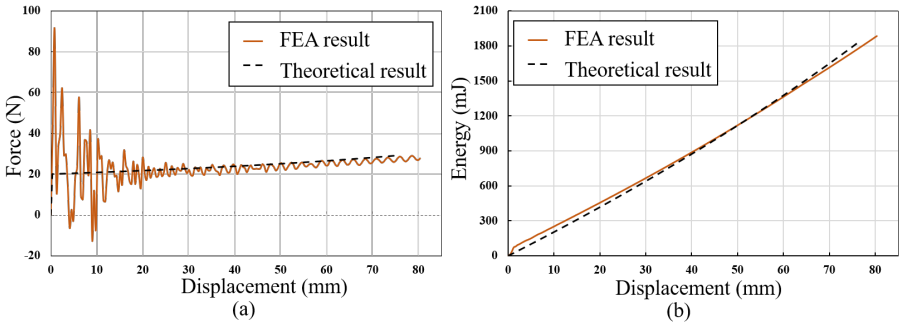


Fig. 11. (a) Force-displacement curves of both theoretical result and simulation result of outward folding RC-kiri. (b) Energy-displacement curves of outward folding RC-kiri.

5 Conclusion

This paper focuses on the compressive motion of kirigami and applies it to transform the non-rigid foldability of some tubular origami structures. Multiple configurations are

generated using the kirigami technique, which has broad applications in many fields, including robotics, mechanical metamaterials, and medical devices. Meanwhile, we also introduce the commonly used outside LET joints to the tubular RC-kiri. Kinematic analysis and static analysis are carried out to obtain the force-displacement relationships. The finite element simulation is carried out by Abaqus, and the results are compared with the theoretical curves, which are in good agreement. The errors between the simulation and theoretical results are also analysed. The accuracy of the theoretical model is verified by tracing the dihedral angles, measuring the diameter and analysing the outward folding configuration. A physical model is manufactured by 3D printing, and further experiments will be conducted in the future.

APPENDIX

Video:https://youtube.com/shorts/rA1cRoIcpNc

References

1. Sargent, B., Butler, J., Seymour, K., Bailey, D., Jensen, B., Magleby, S., Howell, L.: An Origami-Based Medical Support System to Mitigate Flexible Shaft Buckling. Journal of Mechanisms and Robotics **12**(4) (03 2020). https://doi.org/10.1115/1.4045846, 041005
2. Paez, L., Agarwal, G., Paik, J.: Design and analysis of a soft pneumatic actuator with origami shell reinforcement. Soft Robotics **3**(3), 109–119 (2016). https://doi.org/10.1089/soro.2016.0023
3. Wu, S., Ze, Q., Dai, J., Udipi, N., Paulino, G.H., Zhao, R.: Stretchable origami robotic arm with omnidirectional bending and twisting. Proceedings of the National Academy of Sciences **118**(36), e2110023118 (2021). https://doi.org/10.1073/pnas.2110023118
4. Energy absorption of origami tubes with polygonal cross-sections. Thin-Walled Structures **157**, 107013 (2020). https://doi.org/10.1016/j.tws.2020.107013
5. Zhai, Z., Wang, Y., Jiang, H.: Origami-inspired, on-demand deployable and collapsible mechanical metamaterials with tunable stiffness. Proceedings of the National Academy of Sciences **115**(9), 2032–2037 (2018). https://doi.org/10.1073/pnas.1720171115
6. Ye, S., Zhao, P., Zhao, Y., Kavousi, F., Feng, H., Hao, G.: A novel radially closable tubular origami structure (rc-ori) for valves. Actuators **11**(9) (2022). https://doi.org/10.3390/act11090243
7. Miura, K., Tachi, T.: Synthesis of rigid-foldable cylindrical polyhedra (2011)
8. Bös, F., Wardetzky, M., Vouga, E., Gottesman, O.: On the incompressibility of cylindrical origami patterns. Journal of Mechanical Design **139**(2) (12 2016). https://doi.org/10.1115/1.4034970, 021404
9. Tachi, T., Miura, K.: Rigid-foldable cylinders and cells (2013)
10. Butler, J., Morgan, J., Pehrson, N., Tolman, K., Bateman, T., Magleby, S.P., Howell, L.L.: Highly compressible origami bellows for harsh environments. International Design Engineering Technical Conferences and Computers and Information in Engineering Conference, vol. Volume 5B: 40th Mechanisms and Robotics Conference (08 2016). https://doi.org/10.1115/DETC2016-59060
11. Melancon, D., Forte, A.E., Kamp, L.M., Gorissen, B., Bertoldi, K.: Inflatable origami: Multimodal deformation via multistability. Advanced Functional Materials **32**(35), 2201891 (2022). https://doi.org/10.1002/adfm.202201891

12. Pagano, A., Yan, T., Chien, B., Wissa, A., Tawfick, S.: A crawling robot driven by multi-stable origami. Smart Materials and Structures **26**(9), 094007 (aug 2017). https://doi.org/10.1088/1361-665X/aa721e
13. Jin, L., Forte, A.E., Deng, B., Rafsanjani, A., Bertoldi, K.: Kirigami-inspired inflatables with programmable shapes. Advanced Materials **32**(33), 2001863 (2020). https://doi.org/10.1002/adma.202001863
14. Rafsanjani, A., Jin, L., Deng, B., Bertoldi, K.: Propagation of pop ups in kirigami shells. Proceedings of the National Academy of Sciences **116**(17), 8200–8205 (2019). https://doi.org/10.1073/pnas.1817763116
15. Delimont, I.L., Magleby, S.P., Howell, L.L.: A Family of Dual-Segment Compliant Joints Suitable for Use as Surrogate Folds. Journal of Mechanical Design **137**(9) (07 2015). https://doi.org/10.1115/1.4030875, 092302
16. Yang, M., Grey, S.W., Scarpa, F., Schenk, M.: Large impact of small vertex cuts on the mechanics of origami bellows (2022). https://doi.org/10.48550/ARXIV.2209.07422
17. Reid, A., Lechenault, F., Rica, S., Adda-Bedia, M.: Geometry and design of origami bellows with tunable response. Phys. Rev. E **95**, 013002 (Jan 2017). https://doi.org/10.1103/PhysRevE.95.013002
18. Hwang, H.Y.: Effects of perforated crease line design on mechanical behaviors of origami structures. International Journal of Solids and Structures **230-231**, 111158 (2021). https://doi.org/10.1016/j.ijsolstr.2021.111158
19. Tachi, T.: Rigid-foldable thick origami (2010)
20. Lang, R.J., Tolman, K.A., Crampton, E.B., Magleby, S.P., Howell, L.L.: A review of thickness-accommodation techniques in origami-inspired engineering. Applied Mechanics Reviews **70**(1) (02 2018). https://doi.org/10.1115/1.4039314, 010805
21. Pehrson, N.A., Magleby, S.P., Lang, R.J., Howell, L.L.: Introduction of monolithic origami with thick-sheet materials. Proceedings of IASS Annual Symposia **2016**(13), 1–10 (2016)
22. Lang, R.J., Magleby, S., Howell, L.: Single Degree-of-Freedom Rigidly Foldable Cut Origami Flashers. Journal of Mechanisms and Robotics **8**(3) (03 2016). https://doi.org/10.1115/1.4032102, 031005
23. Butler, J., Pehrson, N., Magleby, S.: Folding of Thick Origami Through Regionally Sandwiched Compliant Sheets. Journal of Mechanisms and Robotics **12**(1) (10 2019). https://doi.org/10.1115/1.4045248, 011019
24. Yu, J.: State-of-art of compliant mechanisms and their applications. Journal of Mechanical Engineering **51**, 53 (2015)
25. Hao, G., Yu, J., Li, H.: A brief review on nonlinear modeling methods and applications of compliant mechanisms. Frontiers of Mechanical Engineering **11**(2), 119–128 (06 2016). https://doi.org/10.1007/s11465-016-0387-9
26. Delimont, I.L., Magleby, S.P., Howell, L.L.: Evaluating Compliant Hinge Geometries for Origami-Inspired Mechanisms. Journal of Mechanisms and Robotics **7**(1) (02 2015). https://doi.org/10.1115/1.4029325, 011009
27. Xie, Z., Qiu, L., Yang, D.: Design and analysis of outside-deployed lamina emergent joint (od-lej). Mechanism and Machine Theory **114**, 111–124 (2017). https://doi.org/10.1016/j.mechmachtheory.2017.03.011
28. Ferrell, D.B., Isaac, Y.F., Magleby, S.P., Howell, L.L.: Development of criteria for lamina emergent mechanism flexures with specific application to metals. Journal of Mechanical Design **133**(3) (03 2011). https://doi.org/10.1115/1.4003538, 031009
29. Wilding, S.E., Howell, L.L., Magleby, S.P.: Introduction of planar compliant joints designed for combined bending and axial loading conditions in lamina emergent mechanisms. Mechanism and Machine Theory **56**, 1–15 (2012). https://doi.org/h10.1016/j.mechmachtheory.2012.05.007

30. Sun, Y., Ye, W., Chen, Y., Fan, W., Feng, J., Sareh, P.: Geometric design classification of kirigami-inspired metastructures and metamaterials. Structures **33**, 3633–3643 (2021). https://doi.org/10.1016/j.istruc.2021.06.072
31. Morikawa, Y., Yamagiwa, S., Sawahata, H., Numano, R., Koida, K., Ishida, M., Kawano, T.: Ultrastretchable kirigami bioprobes. Advanced Healthcare Materials **7**(3), 1701100 (2018). https://doi.org/10.1002/adhm.201701100
32. Brooks, A.K., Chakravarty, S., Ali, M., Yadavalli, V.K.: Kirigami-inspired biodesign for applications in healthcare. Advanced Materials **34**(18), 2109550 (2022). https://doi.org/10.1002/adma.202109550
33. Park, J.J., Won, P., Ko, S.H.: A review on hierarchical origami and kirigami structure for engineering applications. International Journal of Precision Engineering and Manufacturing-Green Technology **6**(1), 147–161 (2019)
34. Pneumatic Extension Actuators With Kirigami Skins, Smart Materials, Adaptive Structures and Intelligent Systems, vol. ASME 2020 Conference on Smart Materials, Adaptive Structures and Intelligent Systems (09 2020). https://doi.org/10.1115/SMASIS2020-2219, v001T08A001
35. Babaee, S., Shi, Y., Abbasalizadeh, S., Tamang, S., Hess, K., Collins, J.E., Ishida, K., Lopes, A., Williams, M., Albaghdadi, M., et al.: Kirigami-inspired stents for sustained local delivery of therapeutics. Nature Materials **20**(8), 1085–1092 (2021)
36. Suh, J.E., Kim, T.H., Han, J.H.: New approach to folding a thin-walled yoshimura patterned cylinder. Journal of Spacecraft and Rockets **58**(2), 516–530 (2021). https://doi.org/10.2514/1.A34784
37. Tachi, T.: Simulation of rigid origami. Origami 4: Fourth International Meeting of Origami Science, Mathematics, and Education **4** (08 2009). https://doi.org/10.1201/b10653-20
38. Bowen, L., Baxter, W., Magleby, S., Howell, L.: A position analysis of coupled spherical mechanisms found in action origami. Mechanism and Machine Theory **77**, 13–24 (2014). https://doi.org/10.1016/j.mechmachtheory.2014.02.006
39. Hull, T.: Project Origami: Activities for Exploring Mathematics (04 2013). https://doi.org/10.1201/b10689
40. Chen, G., Magleby, S.P., Howell, L.L.: Membrane-enhanced lamina emergent torsional joints for surrogate folds. Journal of Mechanical Design **140**(6) (04 2018). https://doi.org/10.1115/1.4039852, 062303
41. Roark, R.J., Young, W.C., Plunkett, R.: Formulas for stress and strain (1976)
42. Jacobsen, J.O., Chen, G., Howell, L.L., Magleby, S.P.: Lamina emergent torsional (let) joint. Mechanism and Machine Theory **44**(11), 2098–2109 (2009). https://doi.org/10.1016/j.mechmachtheory.2009.05.015